Progress In Electromagnetics Research, Vol. 126, 237–254, 2012

INEXPENSIVE AND EASY FABRICATION OF MULTIMODE TAPERED DIELECTRIC CIRCULAR PROBES AT MILLIMETER WAVE FREQUENCIES

B. Zhu*, J. Stiens, V. Matvejev, and R. Vounckx

Laboratory for Micro-and Photon Electronics, Department of Electronics and Informatics, Vrije Universiteit Brussel Plainsman 2, Brussels 1050, Belgium

Abstract—Tapered dielectric fibers are widely used in the near field microscopy to focus the incident beam or collect near field signal. Single mode is always required so that the geometrical dimension of the waveguide is smaller than the wavelength. This paper proposes an inexpensive and easy fabrication of multimode tapered Teflon probe which has bigger dimensions than the wavelength. The field distribution in and outside the probe is analyzed by the total internal reflection theorem and solid core circular dielectric waveguide theory. Simulations are carried out in Microwave Studio CST. Novel applications based on focal points in and outside the probe are discussed, especially dielectric permittivity sensing of biomolecules using a capillary tube is emphasized by the simulations and experiments.

1. INTRODUCTION

Tapered dielectric waveguides have been extensively used since 1970s in designing components in millimeter, sub-millimeter and optical circuitry. Many papers have been published in analyzing various formulations of the coupled mode theory and their use in different applications. There also exists a vast amount of literatures on the methods for analyzing the propagation of electromagnetic fields in longitudinally uniform waveguide structures which support eigen modes of the guide. Causa et al. proposed computation of propagation in adiabatically tapered dielectric structures based on eigenfunction

Received 2 January 2012, Accepted 23 February 2012, Scheduled 17 March 2012
* Corresponding author: Bin Zhu (bzhu@etro.vub.ac.be).

expansions in [1]. Coupling of modes on a tapered dielectric cylinder was analyzed by Snyder in [2]. Kobayashi and Mittra developed tapered dielectric rod antennas of rectangular cross section in millimeter wave dielectric integrated circuits in [3]. De and Attimarad performed accurate numerical solutions using Ritz-Galerkin variational approach with appropriate sets of expanding functions to obtain the scattering parameters of the two dimensional tapered dielectric waveguide in [4]. Choudhury and Soon Presented a three-layer tapered core liquid crystal optical fiber and TE mode propagation through it in [5]. Zheng thoroughly elaborated the understanding of the radiation from dielectric tapers when the tapered angle is small and the material is lossless in [6]. Papakonstantinou et al. coded with multimode polymer bent tapered waveguide modeling and got better lateral alignment in [7]. Choudhury and ing dealt with the dispersion relations of tapered core optical fibers with liquid crystal clad in [8]. In most of these cases waveguides with only one or few guided modes are handled and the tapering angle is very small. Soenmez et al. analyzed highly multimode tapered dielectric waveguides and used them to focus light and increase of the tolerance towards vertical and lateral misalignments [9]. Adam comprehensively concluded near field Terahertz measurements and their applications in [10]. Normally, small tapering angle single mode waveguides are used in the near field optic microscopy to guide the wave directly to the sample or collect the near field signal. The dimensions of the tapered waveguides are always smaller than the propagating wavelength. An advanced technique is required and it is difficult to make cheap components.

This paper deals with the full range of angles of the multimode tapered dielectric probe. The total internal reflection theorem and solid core circular dielectric waveguide theory are introduced in Section 2. Focal points in and outside the probe are traced beyond example. The E-field distributions in and outside the probe is simulated in microwave studio CST in Section 3. The influence of geometrical parameters of the tapered dielectric probe is illustrated. Applications are discussed in Section 4. Near field applications such as illuminating and detecting in the near field have been reported using the focal beam outside the probe. A dielectric permittivity of biomolecules sensor application is underlined using the focal point inside the probe. A tapered probe with a hole at the position of the inside focal point is designed for a capillary tube with different liquids in it. Water and methanol in different diameter capillary tubes are simulated, reflection parameters are analyzed. An experimental setup based on an MVNA (Millimeter wave Vector Network Analyzer) is built and the results are shown. Conclusions are drawn in Section 5.

2. TAPERED CIRCULAR DIELECTRIC WAVEGUIDE THEORY

Figure 1(a) shows the geometry of a solid core circular dielectric tapered cylinder. A circular dielectric cylinder of radius a with permittivity ε_1 and permeability μ_0 is immersed in an infinite medium with permittivity ε_2 and permeability μ_0, here $\varepsilon_1 > \varepsilon_2$. Fig. 1(b) depicts the cone tip and defines geometrical parameters in the Cartesian x, y, and z coordinate system, whereby z is assumed to be along the taper axis: cylinder radius R, length L and cone angle α. The tapered cone can be considered as it is formed with a huge number of infinitely thin cylinders ($\Delta z \to 0$) with successively decreasing radii.

Figures 2(a), (b), (c) show what happen when the electromagnetic waves (plane waves) strike the interface of tapered cone for different tapering angles. Suppose that a parallel light beam propagates along the z direction, α_c is the supplementary angle for the critical angle

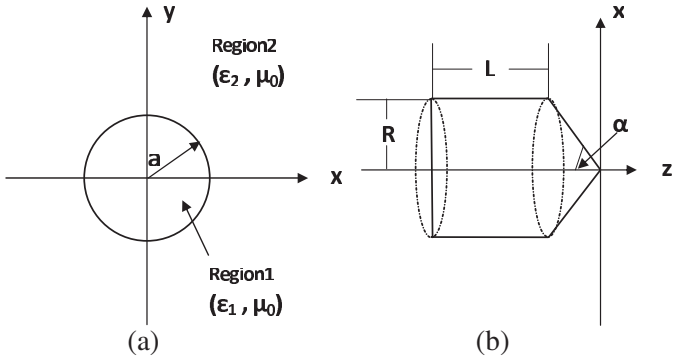

Figure 1. (a) is geometry of a solid core circular cylinder immersed in an infinite medium and (b) is the analysis model of a tapered dielectric probe.

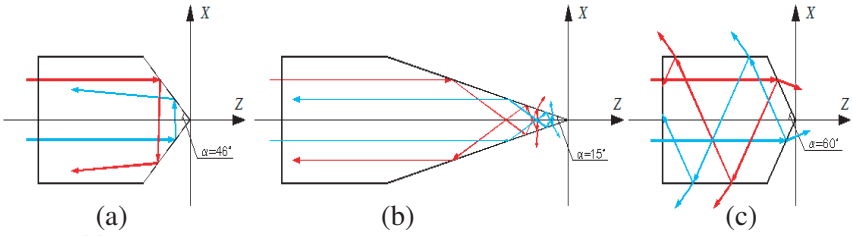

Figure 2. The total internal reflection (a) is for $\alpha = \alpha_c$ (b) is for $\alpha < \alpha_c$ (c) is for $\alpha > \alpha_c$.

of the incident beam. When tapering angle $\alpha \leq \alpha_c$, the total internal reflection phenomenon happens and the beam bounces on the interface until the incident angle is smaller than the critical angle which is close to the end of the tip. On the other hand, refraction occurs and transmitted wave goes out of the cone when $\alpha > \alpha_c$. Many bounced overlying beams create focal points inside and transmitted refraction beams yielding focal points outside the probe.

In this study, the propagation dielectric waveguide theory is used to explain the operation of tapered dielectric probes. The field distribution inside and outside the cylinders can be analytically expressed as demonstrated in [11] chapter 5.

Equations in region 1 and 2 indicate that Bessel functions of the first kind impact the field distribution in region 1, the modified Bessel functions of the second kind influence region 2, respectively. For the tapered dielectric probe, as can be seen from Fig. 1(b), the cone part can be treated as a set of solid cylinders with small length Δz and with successively decreased $R \to 0$. Only the HE_{11} mode, the dominant mode has zero cutoff frequency. For a Teflon single mode operation probe, $a \leq 1.2\,\text{mm}$ is the single mode condition. If $a > 1.2\,\text{mm}$, high order modes exist in the probe and gradually disappeared in tapered conical part. Single mode is possible in the end of the tapered cone, $0 < a < 1.2\,\text{mm}$.

Zheng explained that the light beam in a single-mode dielectric taper establishes a field that is evanescent outside the taper core when the tapering angle is small and the energy radiated from the taper interior is concentrated in the close vicinity of the taper core for the whole length of the taper, no matter how long the taper is, whereas the radiation loss is found to be of second order in the tapering angle in [6]; Paying more attention to the description of circular taper, equation 47 in that paper manifests that the local fundamental mode is in accordance with the previous supposition, and that the Bessel function of the first kind of order n and modified Bessel function of the second kind of order n determine the field inside and outside the taper, respectively. It is emphasized that the results are valid only when the tapering angle is small and the normal distance to the taper core (r) is large. What Zheng explained in that paper is about optic single mode tapered fiber. The radius of the fiber and the tapering angle should be small, it is single mode. It can be observed from Fig. 2(b) when the angle is smaller, the transmitted refraction outside the cone is close to the end of the tip. When the radius is bigger than 1.2 mm, higher order modes are supported in the cylinder part and the higher order modes can not be guided anymore when the waveguide becomes narrow, the power of this mode is coupled into the radiation

modes and decreases abruptly. Lower modes can be guided and at the end of the tip, only HE_{11} mode exists.

3. SIMULATION ANALYSIS

CST Microwave Studio is a general-purpose electromagnetic simulator based on the Finite Integration Technique (FIT). All the simulations in this work are done in the time domain and supposed that all the probes are made of Teflon (lossy $\varepsilon_r = 2.08$, $\tan\delta = 0.0002$) at 100 GHz. Radius $R = 9$ mm, length $L = 9.75$ mm, and variable angles α are simulated to see the influence inside and outside the probe. A plane wave in open boundary conditions is set with default Gaussian exciting source which is a broadband Gaussian pulse signal in the time domain in all the simulations.

The cone angle plays an important role as concluded in previous section, since it determines the radius of limited small cylinder modes. When the angle is small, it can be observed from Fig. 3 that the vast majority of the energy is inside the probe. The boundary condition a in Fig. 1(a) changed with the cone angle. When angle α is increasing, a decreases at the same distance in the z direction, the same point in region 1 will go to region 2. The initial E-field intensity for region 2 is higher than before, therefore, as the side leakage is stronger. This is in agreement with [6], the smaller the tapering angle is, the smaller the radiation angle is and the energy radiated from taper interior can never go far from the taper cone. The higher order modes can also propagate in the cone until the diameter could not support it. More bounced reflection beams overlying inside the probe. Internal focal points are created by these overlying beams. The focusing area is wide, especially when the tapering angle is very small.

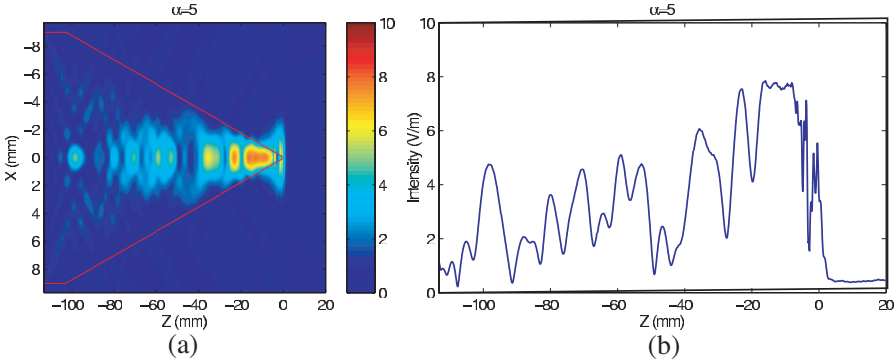

(a) (b)

Figure 3. E-field distribution in the xz plane (a) and E-field intensity when $x = 0$ (b) for $\alpha = 5°$.

As calculated, the critical angle of Teflon is 44°, the corresponding probe tapering angle is 46°. E-field distributions are shown in Fig. 4 for tapering angle $\alpha = 40°, 45°, 48°, 50°$. When $\alpha < 46°$, total internal reflection happens and less side leakage. The beam starts to come out when $\alpha > 46°$. The focusing area inside the cone is narrower than in Fig. 3 and the focusing points converge to the end of the tip, the side leakage and the intensity of the focusing point outside the probe increase when the angle α is increasing.

As can be seen from Fig. 5 for $\alpha = 60°$, the energy is mainly outside the probe and the probe acts like a lens. The bounced reflected overlying beams are decreasing and the transmission increases when the angle α is increasing. Higher order modes stop faster and more energy transmits outside as side leakage.

Conclusions can be drawn via the full range analysis of the tapering angle simulations from Figs. 3, 4 and 5. When $\alpha \ll \alpha_c$, the main energy is inside the probe and there are evanescent waves close to the tip but no big radiation outside. The focusing area inside is larger if the angle is smaller and the focal points come closer to the tip when the angle is increasing. When $\alpha \gg \alpha_c$, the focal point outside the probe is more obvious and the symmetrical side leakage in multiple lobes is stronger than for small tapering angles. For α is around α_c, there are mainly two peaks inside the cone, the distance between these two peaks gets smaller when α is increasing and the position of the maximum peak shifts around 1 mm. In this range of angles, where two peaks exist inside the cone, the tapering angle is not critical which is a big advantage for the inexpensive and easy fabrication application in dielectric permittivity sensing.

The radius R is very important since it determines the boundary conditions in region 1 and 2 and it also affects the mode propagation inside the probe. When R is bigger than the single mode conditions, 1.2 mm in this case, higher order modes exist and bounce until the cone radius can not support them. The focal points inside and outside are the results of interactions between all these modes. It is difficult to find the regularity for these focal points. Finally we choose $R = 9$ mm as a reasonable value. By changing L, the length of the cylinder part, phase and loss are changed as Teflon is lossy material. The frequency and the dielectric permittivity of the cone material also influence the E-field distribution as the critical angle is wavelength and material dependent.

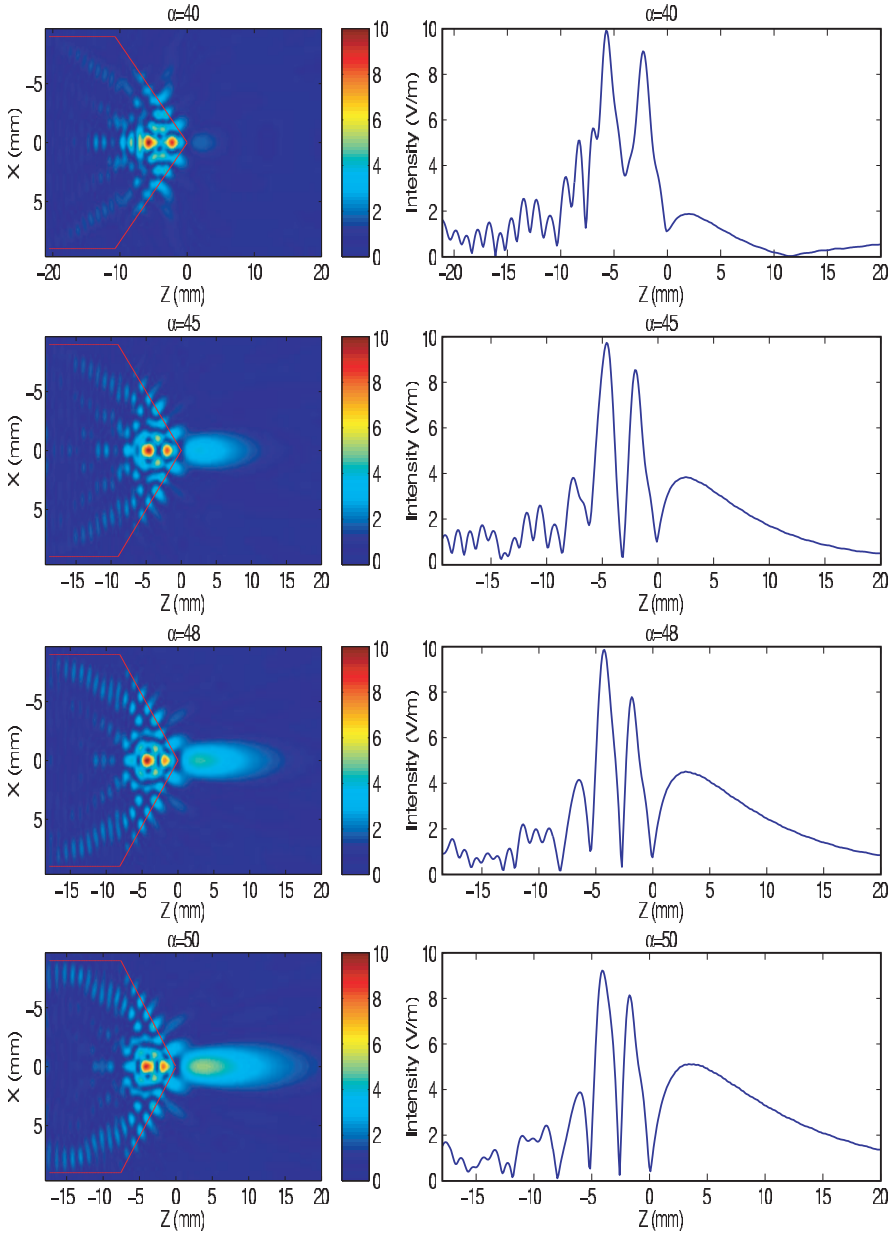

Figure 4. E-field distribution in the xz plane (a) and E-field intensity when $x = 0$ (b) for $\alpha = 40°$, $\alpha = 45°$, $\alpha = 48°$, $\alpha = 50°$.

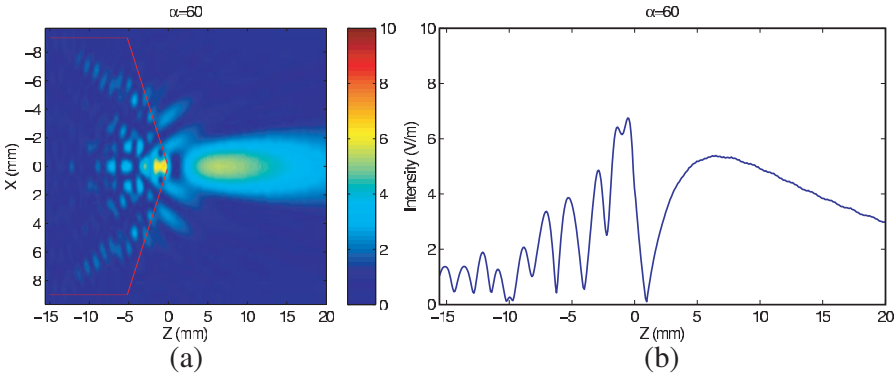

Figure 5. E-field distribution in the xz plane (a) and E-field intensity when $x = 0$ (b) for $\alpha = 60°$.

4. APPLICATION DISCUSSION

Small angle single mode tapered dielectric probes are widely used in near-field applications for illuminating and collecting the near field signal. Tapered probes with angles bigger than the critical angle can act as axicons and can be applied as illuminating probes. In previous publications [12–14], optimal results for the tapered probe were obtained from Cassandra simulations which is a three-dimensional full-wave simulation packages at UGent [15]. In these simulations, the dielectric tapered probe was used as an illumination probe and also as a detection probe in a near-field millimeter and terahertz wave microscope. The advantage of using a tapered probe is increasing the tolerance towards vertical and lateral misalignments there as illustrated in [9].

Near field applications use the focal point outside the probe, the probe angle is always around or a little bigger than the probe critical angle. Using the focal point inside the probe opens the door for the development of novel applications such as dielectric permittivity sensing of biomolecules. As is well known, numerous research publications prove that Terahertz waves can probe various inter and intra-macromolecular functional properties: biomolecules' [16] and lipid membrane's hydration [17], binding reactions with other biomolecules [18], conformational changes [19] and its functioning [20]. Matvejev et al. proposed a highly sensitive integrated waveguide structure for nano-liter liquids in capillary tubes [21, 22]. Bulk wet anisotropic etching and micromachining are used to pattern a small hole for inserting a capillary tube. The same kind of capillary tubes are used in this paper and inserted into the focusing position inside

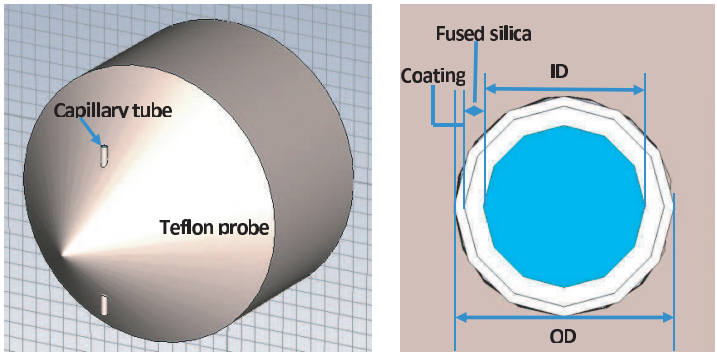

(a) (b)

Figure 6. (a) A capillary tube is inserted into a tapered probe, (b) is the geometrical dimension of a capillary tube.

the taper.

The optimal position of the probe is dependent on the dielectric characteristics of the cone material. If the material is hard, it is easy to pattern the hole close to the tip, but if the material is soft like Teflon, it is better to keep it far from the tip. In this study, we use Teflon and it is observed from Fig. 4 that $\alpha = 40^\circ$ is the best compromise. The E-field intensity is highest at the first focal point ($z = -5.88\,\text{mm}$) which is relatively far from the end of the tip, the hole is easy to make by mechanical tools. Fig. 6(a) shows a teflon probe with an inserted capillary tube, (b) shows the geometrical dimensions of a capillary tube, where OD is the outer diameter and ID is inner diameter. The capillary tubes are from Polymicro Technologies with standard polyamide coating ($\varepsilon_c = 3.5$, $\tan\delta = 0.0027$ from CST library), synthetic fused silica tube ($\varepsilon_{fs} = 3.75$, $\tan\delta = 0.0004$ from CST library). The dielectric permittivity parameters for water and methanol are referred from [21] and [23] in the form of the 2nd order Debye model which is shown in Table 1, where ϵ_{inf} is Epsilon infinity, ϵ_{s1} is Epsilon static 1, ϵ_{s2} is Epsilon static 2, Rt_1 is relaxation time 1, and Rt_2 is relaxation time 2. In the following simulations where we vary the dimension of the capillary tube and the liquid content (water and methanol) in it, we position the edge of the capillary tube at $z = -5.88\,\text{mm}$.

The incident wave is assumed as a plane wave, which is emitted from the cylinder part at XY plane, and the reflection parameters (S_{11}) are detected at the beginning plane of the cylinder part. This modeling approach is different from the single mode waveguide introduced in [21]. Not only the amplitude of S_{11}, but also the shape of the standing wave is sensitively dependent on the permittivity of the liquid inside the

Table 1. The 2nd order Debye model for methanol and water.

Sample	ϵ_{inf}	ϵ_{s1}	ϵ_{s2}	Rt_1	Rt_2
Methanol	2.79	32.50	5.91	$51.5e-12$	$7.09e-12$
Water	4.59	77.97	6.18	$8.32e-12$	$1.02e-12$

Table 2. Geometrical dimensions for different capillary tubes.

Product descriptor	ID (μm)	OD (μm)	Coating (μm)
TSP100375	100 ± 04	363 ± 10	20
TSP320450	320 ± 06	435 ± 10	18
TSP700850	700 ± 10	850 ± 20	24

capillary.

Table 2 shows the information about the dimension of the capillary tube used in the simulations. Simulations were executed for the average ID and OD dimensions indicated in Table 2. Fig. 7 shows the simulation results for different tubes with water and methanol or air in them. The frequency is swept from 50 to 300 GHz.

As the shape of the standing wave is dependent on the dielectric permittivity of the liquid inside the capillary tube, the amplitude and phase of S_{11} will express this sensitivity as well. It can be observed from Fig. 7 that this standing wave interference pattern is very sensitive to the path length and hence to a very small variation in the dielectric permittivity of the liquid materials. The wavelength inside the liquid gets smaller when the sweeping frequency is increasing (1.5 mm to 450 μm for water and 3.3 mm to 600 μm for methanol when the frequency is sweeping from 50 to 300 GHz). Compared with Figs. 7(a), (c) and (e), There are big differences between water, methanol and air when ID is wider as the inner dimension of the capillary tube becomes comparable with the propagating wavelength in the liquids. For the larger ID (320, 720 μm), the standing wave interference pattern is more sensitive to the content of the capillary tube. It is more clear to see the difference between water and methanol from (b), (d), (f). It is less sensitivity in (f) when ID is smaller and especially in the lower frequency range. Assuming that the integrated area of δS_{11} over the considered frequency range can express the sensitivity over the whole band, (d) shows that when $ID = 320$ μm, this integrated area is the biggest; (f) $ID = 700$ μm has the biggest δS_{11} value at some frequency ($f = 244.75$), but the area is smaller than that in (d), no big improvement in terms of sensitivity in the whole band.

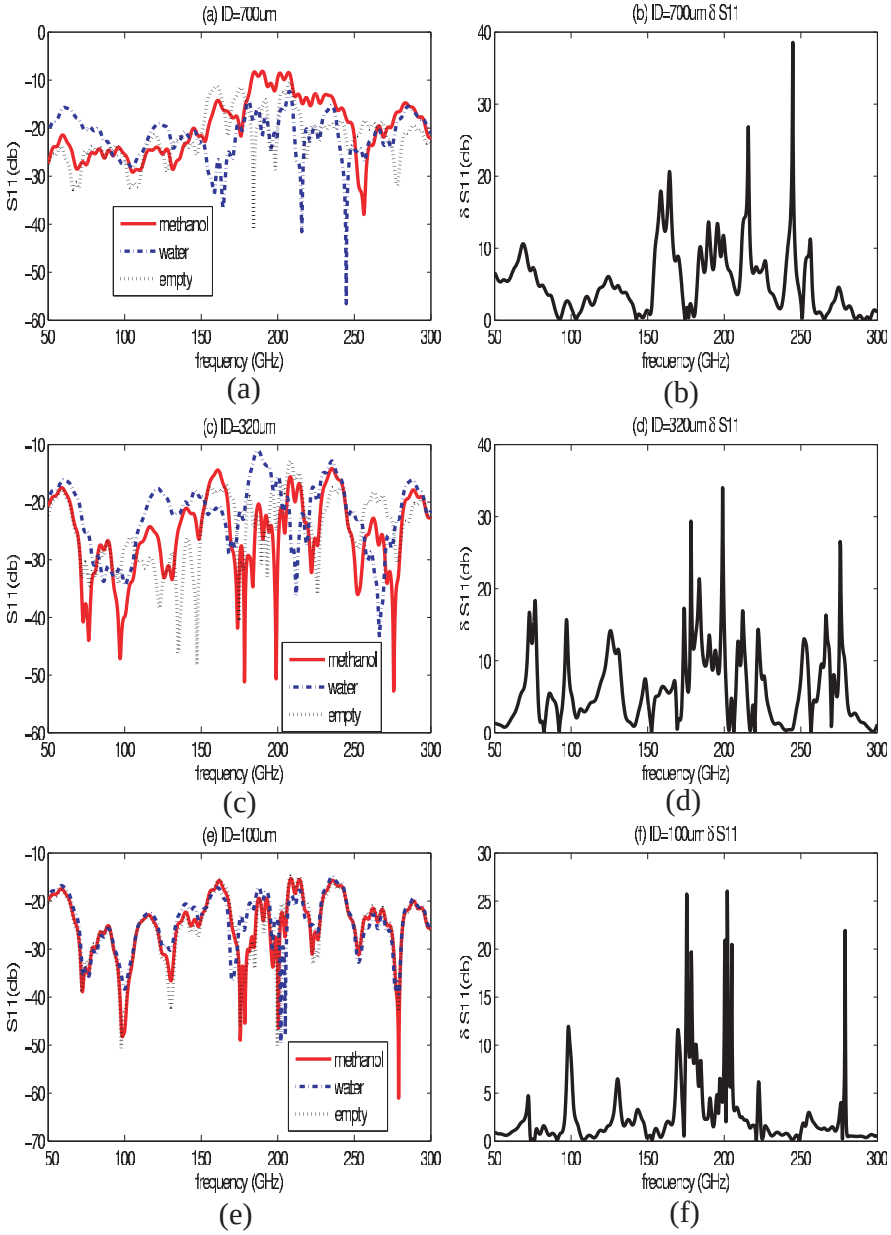

Figure 7. (a), (c), (e) are the simulation results for different liquids in the capillary tube, (b), (d), (f) are the absolute differences for water and methanol when $ID = 700$, 320 and 100 µm.

Details about the E-field distribution in the tube with water and methanol ($ID = 700\,\mu m$) are shown in Fig. 8. $f = 265.25\,GHz$, $f = 244.75\,GHz$ is the lowest δS_{11} value for methanol and water; $f = 190\,GHz$, $f = 207.75\,GHz$ is the highest δS_{11} value for methanol and water, respectively. Obviously, water is difficult to be penetrated (black lines are the position of the capillary tube.) and there are focal points inside the tube for methanol. The E-field intensity of the highest δS_{11} value at $f = 190$, $207.75\,GHz$ is stronger than that of the lowest δS_{11} value for water and methanol, which is in line with the theory.

It is difficult to explain each inflection point for the considered multimode tapered probe. The standing wave is not regular like

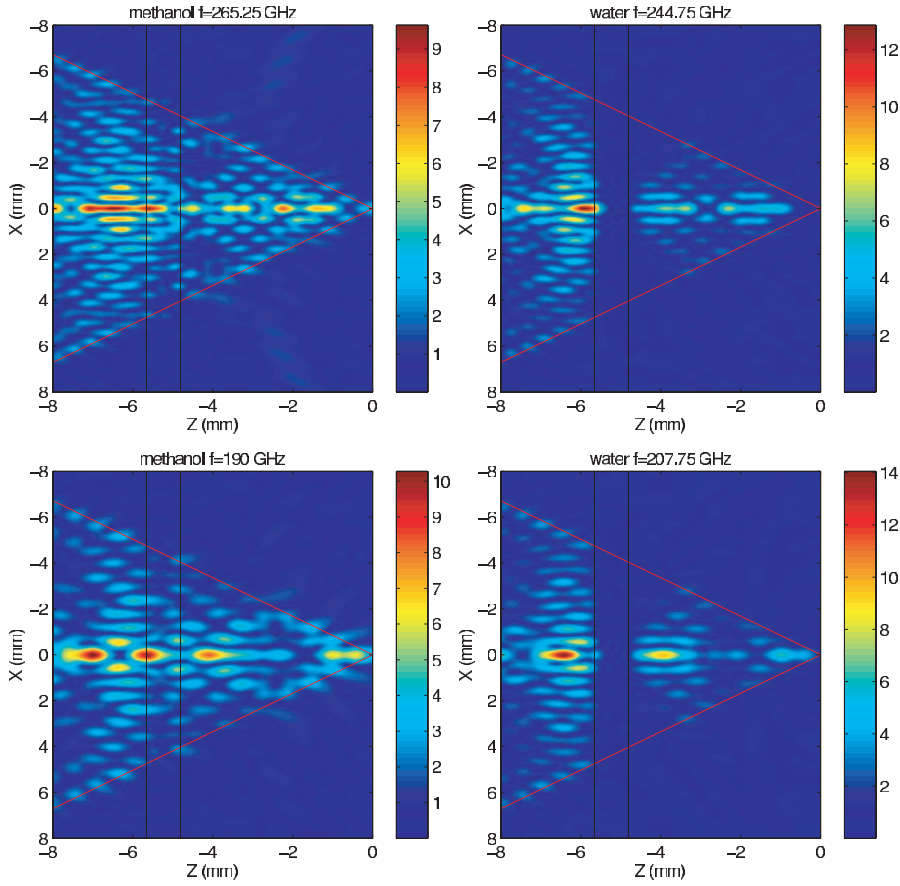

Figure 8. E-field distribution for water and methanol in the capillary tube at resonant frequency and non-resonant frequency ($ID = 700\,\mu m$).

the results from [21] with single mode. It is a good idea to use this easy fabrication multimode tapered probe to Characterize solved biomolecules in the database.

Experimental setup was built based on an MVNA in Fig. 9, a 40° tapered Teflon probe with a 1 mm hole was used as well as a capillary tube of 363 µm outer diameter was used (bigger diameter capillary tubes would be more ideal but not available). The waves coming out from the corrugated horn antenna can be treated as plane waves in the far field. The source part can be replaced by other millimeter wave emitter instead of an MVNA to reduce the costs. This setup was fixed at W-band (70–110 GHz).

In order to compare the experimental data with simulation results, we modified the model of Fig. 6 by introducing an aerial space between the 'too small' capillary tube and the drilled hole. 1 mm diameter hole is set and the left edge is at $z = -5.88$ mm. The 363 µm outer diameter capillary tube is placed in the center, close to the left edge (close to the source in the z direction), right edge (close to the end of the tip in the z direction), front edge (in the y positive direction) or back edge (in the y negative direction) which have been shown in Fig. 10.

It is observed from the simulation results that the position of the capillary tube has a substantial impact on the field distribution. Fig. 11(a) shows the difference between methanol and water (δS_{11}) in different positions, The biggest distinction is observed when the capillary tube is in the left position and the smallest distinction is obtained when the capillary tube is in the right position. The shapes of δS_{11} in the center, front and back positions are similar and since the front and the back are in the same z position with the center position and they are symmetrical, the results are overlaying. As concluded the shifting in the z direction has higher impact factor on the E-field distribution and the shifting in the y direction has slight differences. The air in the hole is 8 times of the capillary tube. The reflection on the

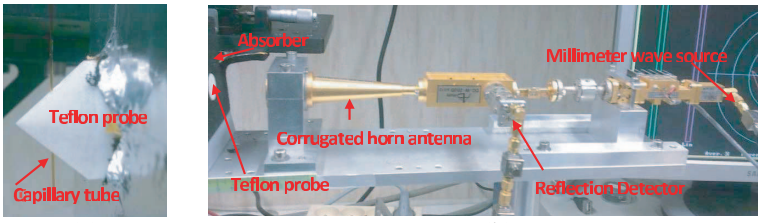

(a) (b)

Figure 9. Experimental setup (a) is a Teflon probe with a capillary tube (b) is the plane wave source and reflection detector.

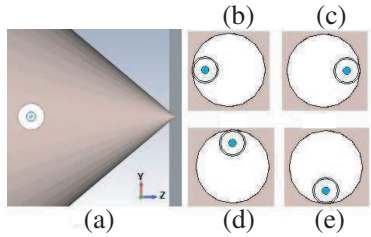

Figure 10. Top view in the yz plane, the capillary tube is (a) in the center position, (b) the left position, (c) the right position, (d) the back position, (e) the front position.

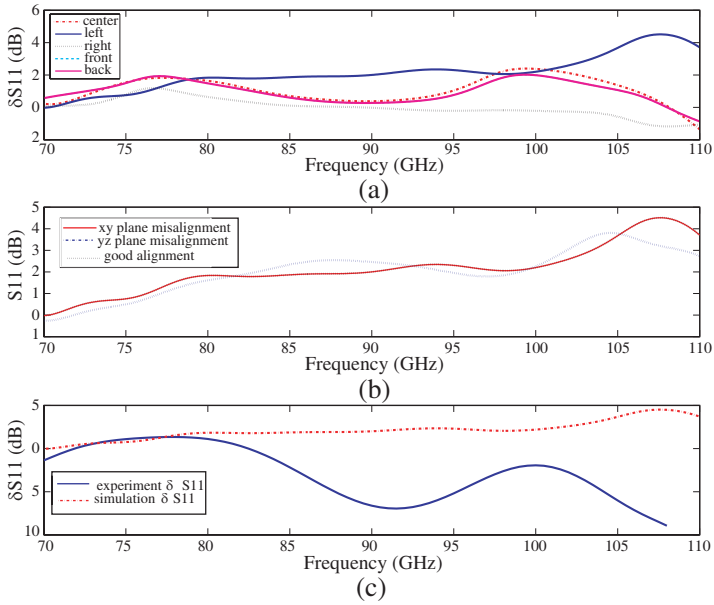

Figure 11. (a) simulated δS_{11} for different capillary positions. (b) 5° misalignment in the xy plane and the yz plane when the capillary is in the left position. (c) comparison of the experimental and simulated δS_{11} when the capillary is in the left position.

edge of the hole decease the waves going through the hole. Compared with Fig. 7(f), we found that mismatched system (the hole size is not the right size of the capillary) is less sensitive than the matched system, 7.5 dB difference. Fig. 11(b) depicts how the misalignment of the tapered tube influence the field distribution when the capillary tube fixed in the left of the hole. 5° misalignment in the xy plane

and the yz plane. It is obvious that the xy misalignment does not impact the field distribution because of the symmetrical structure and the yz misalignment affects the system sensitivity. The capillary tube was fixed in the left position of the hole in the experiments and the data are fitted smoothly without any calibration. Compared with the simulation data δS_{11} when the capillary is in the left position in (c), experimental data curve is not comparable with the simulation data. The problem maybe cause by the misalignment and the bending of the capillary tube. Since the capillary is soft, it is possible to lead the bending inside the hole when fixed the syringe which is connected with the capillary tube and used to inject liquid in the capillary tube. Only the top of the capillary tube was fixed, its position may be changed each time when injecting the liquid. Bending to the right position and the yz misalignment result in the present experimental results. For the sake of obtaining the repeatable experimental results, the syringe is well fixed to avoid the movement position shift when injecting to the capillary tube or refilling itself. The position shift in the z direction leads a substantial influence and the position shift in the y direction impacts less. When we fixed the syringe well on the optic table and sealed the capillary tube with the syringe very well, vibration can be decreased. the experiment is reproducible. If the capillary tube is full of liquid and nothing changed, the experimental results are absolutely repeatable, the difference of each time measurement is less than 0.1 dB. Fig. 12 shows that five times different situation measurements for water. $M1$ is the first experiment result, $M2$ is injecting more water to the capillary tube, $M3$ is refilling new liquid (water) in the syringe and injecting again to update the liquid in the capillary tube. $M4$ is refilling the syringe again. $M5$ is injecting to the capillary tube again. It is observed that 5 times measurements are close to each other and

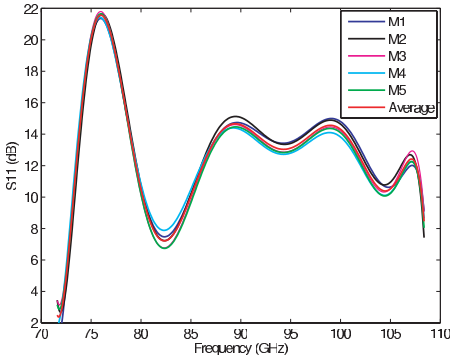

Figure 12. Five times measurements S_{11} for water in different situations and their average result.

keep the same shape. the biggest difference for these measurements is around 1 dB.

This setup is strongly dependent on stable fixing. It is impossible to make the hole just right size of the capillary tube like the simulation, no air gap between hole and capillary tube. Improvement can be designed by integrating the tube and the tapered probe together.

5. CONCLUSIONS

This paper analyzed full range of the multimode tapered dielectric probe angle using the total internal reflection theorem and the solid core circular dielectric waveguide theory. The focal points in and outside the probe were illustrated by microwave studio CST simulation results. Using the focal beam outside the probe when the tapered angle is around or a little bigger than probe critical angle, focusing illumination can be applied. When the angle is smaller than the probe critical angle, focal points inside the probe are associated with the novel application of dielectric permittivity sensing of liquids flowing through a capillary tube inserting in the focal point position. The amplitude and the shape of reflection spectrum reflect the variation of the liquid's permittivity. Capillary tubes having wider inner diameters feature higher sensitivity, but saturate once the diameter is of the order of the $\lambda/4$. Since there is air gap between the hole and the capillary tube in the experimental setup, it is less sensitivity than the simulation. Because the position of the capillary tube in the hole and misalignment in the yz plane also impact the experimental results, we found out the best position is close to the left position. Experimental results showed that the experiments are repeatable. Therefore, A multimode tapered dielectric circular probe is a good inexpensive and easy fabrication solution for these applications at millimeter wave frequencies.

ACKNOWLEDGMENT

This work is funded by the FWO-Vlaanderen project "FWOAL465-Scattering type near-field mm wave microscopy" of the Flemish region in Belgium and is also executed in the framework of NEWFOCUS ESF Research Networking Program (RNP).

REFERENCES

1. Causa, F., J. Sarma, and M. Milani, "Computation of propagation in adiabatically tapered dielectric structures based on eigenfunction expansions: Application to (active) optical devices,"

Antennas and Propagation Society International Symposium, Vol. 2, 762–765, 1997.

2. Snyder, A. W., "Coupling of modes on a tapered dielectric cylinder," *IEEE Transactions on Microwave Theory and Techniques*, Vol. 18, No. 7, 383–392, 1970.
3. Kobayashi, S. and R. Mittra, "Dielectric tapered rod antennas for millimeter-wave applications," *IEEE Transactions on Antennas and Propagation*, Vol. 30, No. 1, 54–58, 1982.
4. De, A. and G. V. Attimarad, "Numerical analysis of two dimensional tapered dielectric waveguide," *Progress In Electromagnetics Research*, Vol. 44, 131–142, 2004.
5. Choudhury, P. K. and W. K. Soon, "TE mode propagation through tapered core liquid crystal optical fibers," *Progress In Electromagnetics Research*, Vol. 104, 449–463, 2010.
6. Zheng, X., "Understanding radiation from dielectric tapers," *JOSA A*, Vol. 6, No. 2, 190–201, 1989.
7. Papakonstantinou, I., D. R. Selviah, and F. A. Fernandez, "Multimode polymer bent tapered waveguide modeling," *Lasers and Electro-Optics Society, LEOS*, Vol. 2, 983–984, 2004.
8. Choudhury, P. K. and P. T. S. Ping, "On the dispersion relations of tapered core optical fibers with liquid crystal clad," *Progress In Electromagnetics Research*, Vol. 118, 117–133, 2011.
9. Soenmez, Y., A. Wallrabenstein, J. Schrage, and G. Mrozynski, "Coupled mode analysis of power transport and loss in highly multimodal tapered dielectric waveguides for coupling applications," *Lasers and Electro-Optics — Pacific Rim, CLEO/Pacific Rim*, Vol. 2, 1–2, 2007.
10. Adam, A. J. L., "Review of near-field terahertz measurement methods and their applications," *International Journal of Infrared and Millimeter Waves*, Vol. 32, 976–1019, 2011.
11. Yeh. C. and I. F. Shimabukuro, *The Essence of Dielectric Waveguides*, Springer, New York, 2008.
12. Zhu, B., J. Stiens, G. Poesen, S. Vanloocke, D. De Zutter, and R. Vounckx, "Dielectric analysis of 3D printed materials for focusing elements operating in mm and thz wave frequency bands," *Proceedings of Symposium IEEE/LEOS Benelux Chapter*, 13–16, Delft, Netherland, 2010.
13. Zhu, B., S. Vanloocke, J. Stiens, D. De Zutter, and R. Vounckx, "A novel 3D Printed focusing probe in scattering-type scanning near-field millimeter and terahertz wave microscope," *European Conference on Antennas and Propagation, EuCAP*, 775–778,

Rome, Italy, 2011.

14. Zhu, B., S. Vanloocke, V. Matvejev, J. Stiens, D. De Zutter, and R. Vounckx, "Scanning near-field millimeter wave microscope combining dielectric tapered probes and metal tips," *PIERS Proceedings*, Vo. 7, No. 6, Suzhou, China, Sept. 12–16, 2011.
15. Peeters, J., J. Fostier, F. Olyslager, and D. De Zutter, "New parallel approaches for fast multipole solvers," *European Conference on Antennas and Propagation, EuCAP*, 5–8, 2007.
16. Leitner, D. M., M. Gruebele, and M. Havenith, "Solvation dynamics of biomolecules: Modeling and terahertz experiments," *HFSP J.*, Vol. 2, 314–323, Dec. 2008.
17. Tielrooij, K. J., D. L. Paparo, H. Piatkowski, J. Bakker, and M. Bonn, "Dielectric relaxation dynamics of water in model membranes probed by terahertz spectroscopy," *Biophys. J.*, Vol. 97, 2484–2492, Nov. 2009.
18. Brucherseifer, M., M. Nagel, P. Bolivar, H. Kurz, A. Bosserhoff, and R. Buttner, "Label-free probing of the binding state of dna by time-domain terahertz sensing," *Appl. Phys. Lett.*, Vol. 77, 4049–4051, Dec. 2000.
19. Markelz, A., S. Whitmire, J. Hillebrecht, and R. Birge, "THz time domain spectroscopy of biomolecular conformational modes," *Phys. Med. Biol.*, Vol. 47, 3797–3805, Nov. 2002.
20. Markelz, A. G., "Terahertz dielectric sensitivity to biomolecular structure and function," *IEEE J. Sel. Top. Quant.*, Vol. 14, 180–190, Jan.–Feb. 2008.
21. Matvejev, V., C. De Tandt, W. Ranson, J. Stiens, R. Vounckx, and D. Mangelings, "Integrated waveguide structure for highly sensitive THz spectroscopy of nano-liter liquids in capillary tubes," *Progress In Electromagnetics Research*, Vol. 121, 89–101, 2011.
22. Matvejev, V., C. De Tandt, W. Ranson, and J. Stiens, "Wet silicon bulk micromachined THz waveguides for low-loss integrated sensor applications," *IEEE 35th International Conference on Infrared, Millimeter, and Terahertz Waves (IRMMW-THz 2010)*, 2, Piscataway, NJ, USA, 2010.
23. Barthel, J., K. Bachhuber, R. Buchner, and H. Hetzenauer, "Dielectric spectra of some common solvents in the microwave region — Water and lower alcohols," *Chem. Phys. Lett.*, Vol. 165, 369–373, Jan. 1990.